Published in final edited form as:
J Nucl Med. 2008 June ; 49(6): 978–986.

Pre-clinical development of a neutral, estrogen receptor-targeted, tridentate ^{99m}Tc(I) estradiol pyridin-2-yl hydrazine derivative for imaging of breast and endometrial cancers

Tapan K. Nayak[1,2], **Helen J. Hathaway**[1,3], **Chinnasamy Ramesh**[4], **Jeffrey B. Arterburn**[3,4], **Donghai Dai**[3,5], **Larry A. Sklar**[2,3,6], **Jeffrey P. Norenberg**[2,3], and **Eric R. Prossnitz**[1,3,*]

1*Department of Cell Biology and Physiology, School of Medicine, University of New Mexico Health Science Center, Albuquerque, NM 87131*

2*College of Pharmacy, University of New Mexico Health Science Center, Albuquerque, NM 87131*

3*Cancer Research and Treatment Center, University of New Mexico Health Science Center, Albuquerque, NM 87131*

4*Department of Chemistry and Biochemistry, New Mexico State University, Las Cruces, NM 88003*

5*Department of Obstetrics and Gynecology, School of Medicine, University of New Mexico Health Science Center, Albuquerque, NM 87131*

6*Department of Pathology, School of Medicine, University of New Mexico Health Science Center, Albuquerque, NM 87131*

Abstract

Breast and endometrial cancers are the most common invasive malignancies in women with more than 217,000 new diagnoses per year in the United States. These cancers are often classified into two subtypes based upon the expression of the classical estrogen receptor (ERα). In this study, we describe a new structural class of neutral tridentate ^{99m}Tc(I)-estradiol-pyridin-2-yl hydrazine derivatives for potential use in breast and endometrial cancer imaging.

Methods—The ^{99m}Tc(I)-estradiol-pyridin-2-yl hydrazine derivative was synthesized using the Sonogashira cross-coupling reaction and radiolabeled using the tricarbonyl approach. Radiochemical purity was assessed by HPLC. Cell binding studies were performed on human breast adenocarcinoma MCF-7 cells. *In vivo* biodistribution of the ^{99m}Tc(I) derivative was performed in virgin female C57BL/6 mice in defined phases of the estrus cycle. Biodistribution and nanoSPECT/CT imaging studies were performed on mice bearing MCF-7 and primary human endometrial tumors.

Results—Radiochemical analysis demonstrated that the post-purification purity of the ^{99m}Tc(I)-estradiol-pyridin-2-yl hydrazine derivative was ≥ 95% with a specific activity of 47.5 TBq ^{99m}Tc/mmol. Cell binding studies yielded a K_d value of 11 ± 1.5 nM. *In vivo* studies revealed that receptor-mediated uptake was present in all phases of the estrous cycle in reproductive organs and mammary glands but was highest during the diestrous phase of the estrous cycle. Despite high non-specific uptake in the liver, significant receptor-mediated uptake was observed in target tissues and ER-expressing tumors (0.67% for MCF-7 tumors and 0.77% for endometrial tumors). Tumor uptake was reduced by approximately 50% upon coinjection with 17β-estradiol.

*Address correspondence to: Eric R. Prossnitz, Department of Cell Biology & Physiology, University of New Mexico, Albuquerque, NM 87131. Tel. 505-272-5647; Fax: 505-272-1421; E-mail: eprossnitz@salud.unm.edu
First author (student): Department of Cell Biology & Physiology, University of New Mexico, Albuquerque, NM 87131. Tel. 505-272-5647; Fax: 505-272-1421; E-mail:tnayak@salud.unm.edu

Disclosure statement: The authors declare no conflicts of interest.

Conclusion—We have characterized a novel neutral tridentate ^{99m}Tc(I)-estradiol-pyridin-2-yl hydrazine derivative for potential use in breast and endometrial cancer imaging. This study is a notable achievement and represents the first step on a path towards the design of estrogen-based Tc-labeled tracers with improved targeting and SPECT-imaging characteristics.

Keywords

Estrogen receptor; small animal SPECT imaging; estrous cycle; breast cancer; endometrial cancer; ^{99m}Tc tricarbonyl

INTRODUCTION

Over 250,000 new cases of breast, ovarian and endometrial cancer were diagnosed in the United States in 2006 (1). Such cancers are often hormonally regulated and can be divided into two subtypes based on whether or not tumor cells express the classical estrogen receptor (ERα). Estrogen promotes cell proliferation and inhibits apoptosis through a complex signaling cascade resulting in transcriptional changes that may include modulation of tumor suppressor function. The presence of ERα in approximately two-thirds of breast cancers correlates with whether the tumor is estrogen-dependent or -independent (2), and represents one of the best prognostic factors in breast cancer due to the availability of anti-estrogens such as tamoxifen and fulvestrant and more recently the aromatase inhibitors. With the recent characterization of a novel transmembrane estrogen receptor, GPR30, in multiple cancer types, the exact causes and mechanisms underlying estrogen-dependence and -resistance in cancers may be more complex than previously appreciated (3-5). Nevertheless, it is clear that if a cancer can be detected at an early stage and characterized for estrogen receptor status and metastatic state, patients display improved outcome with appropriate treatment (6,7). As a result, in the past decade, a greater emphasis has been placed on the development of radiomaging approaches for breast and other cancers using either Single Photon Emission Computerized Tomography (SPECT) or Positron Emission Tomography (PET) (8). Whole body imaging is possible with PET and SPECT and therefore offers a non-invasive approach to assess regional and disseminated cancer.

In 1986, a study involving 547 patients demonstrated the predictive value of determining estrogen-binding activity on the clinical behavior of breast cancer in women (9). Throughout the1980s, a variety of ^{18}F-labeled estrogen derivatives were tested in animals and shown to demonstrate ER selectivity (10,11). The most successful ^{18}F-labeled estrogen derivative, 16α-^{18}F-17β-estradiol (FES), has been evaluated clinically with promising results in imaging estrogen-binding tumors and in predicting responsiveness of breast tumors to anti-estrogen drugs such as tamoxifen (12,13). The role of estrogen in endometrial carcinogenesis has been well documented (14,15) and successful applications of FES have been reported for endometrial and other gynecological cancers (16). Subsequent efforts sought to develop methods for labeling estrogen imaging agents with the widely available and longer-lived radionuclide ^{99m}Tc for SPECT imaging, using both pendant and integrated chelate approaches (17). Reports have described the generation and use of both steroidal and non-steroidal estrogen derivatives labeled with ^{99m}Tc (SPECT) and ^{94m}Tc (PET) for estrogen receptor imaging. However, the agents described to date have demonstrated suboptimal target tissue selectivity *in vivo*, possibly a result of the high lipophilicity or rapid metabolism of these agents. The complex chemistry involved in the radiosynthesis of these compounds in order to obtain high yields and purities has further hampered their development for clinical use (18,19).

We have recently described a new class of neutral tridentate Re-estradiol pyridin-2-yl hydrazine derivatives (see Table 1 in ref. (20)). These compounds were biologically evaluated by competitive radiometric binding assays with ^{3}[H]-estradiol to determine the relative binding

affinities (RBA) to ERα and ERβ. The RBA values compare favorably with the best examples of previously reported estradiol tricarbonyl-Re(I) complexes (8,17,18). Binding to the alternate estrogen receptor, GPR30, was also shown to be of high affinity. A functional assay based on the rapid receptor-mediated mobilization of intracellular calcium elicited by binding to ERα, ERβ or GPR30 revealed that the alkyne-linked complex yielded the highest levels of receptor activation. It has also previously been reported that substitution of a 17α-ethynyl group reduces the affinity of estrogen derivatives for alpha-fetoprotein (AFP) and sex steroid-binding protein resulting in more favorable *in vivo* pharmacokinetics (21,22). In this report, we describe the detailed chemical and biological evaluation of a ^{99m}Tc(I)-estradiol-pyridin-2-yl hydrazine derivative with an alkyne linkage for diagnostic imaging of breast and endometrial cancer.

MATERIALS AND METHODS

Radiosynthesis of ^{99m}Tc(I)-estradiol pyridin-2-yl-hydrazine derivative

The ^{99m}Tc-tricarbonyl complex $[^{99m}Tc(CO)_3(H_2O)_3]^+$ was prepared by adding 3.7 GBq of freshly eluated Na-$^{99m}TcO_4$ to the Isolink® kit reagent (Tyco healthcare, Mallinckrodt, St. Louis, MO, USA) and heating the reaction mixture for 40 min at 100°C. The $[^{99m}Tc(CO)_3(H_2O)_3]^+$ complex was allowed to cool for 20 min on ice. Due to the acid sensitivity of the tertiary propargylic 17β-alcohol of the estradiol chelate, the alkaline mixture was neutralized to pH 7 with acetic acid. The estradiol-pyridin-2-yl hydrazine derivative was prepared as previously described (20). To generate the radiolabeled complex, the estradiol-pyridin-2-yl hydrazine derivative (10 μg, 21.7 nmol)) was added to the neutralized $[^{99m}Tc(CO)_3(H_2O)_3]^+$ complex and the mixture was stirred for 2 hours at room temperature. Heating was avoided to prevent β elimination of the 17β-alcohol.

Inorganic impurities from the Isolink® kit, aqua ions of ^{99m}Tc (if any) and excess ligand were separated by solid phase extraction with C-18 SepPak Plus cartridges (Waters, Milford, MA USA). Impurities and excess ligand were eluted with 4 × 0.5 mL aliquots of 40% ethanol in water. Elution of the ^{99m}Tc-labeled estradiol-pyridin-2-yl hydrazine derivative was accomplished with 4 × 0.5 mL aliquots of 100% ethanol. Reverse phase HPLC was performed pre- and post-purification to assess radiochemical purity using a reverse-phase C-18 column (JT Baker, Phillipsburg, NJ, USA) with a Gamma-ram radiometric detector (INUS Systems Inc., Tampa, FL, USA). The injection volume was 100 μL and the ultra-violet (UV) detector wavelength was 254 nm. The mobile phase (solvent A) consisted of 100% HPLC grade ethanol whereas the stationary phase (solvent B) consisted of 100% HPLC grade water. The elution gradient was 60-70% solvent A over 10 min. followed by 70-100% in 15 min. with a flow rate of 1 mL/min. Specific activity was determined from the integrated peak radioactivity (compensating for the elution profile of the ^{99m}Tc generator and the transient equilibrium between the parent and the daughter radionuclides) and the *UV* absorption using a calibration curve of known quantities of unlabelled compound.

Stability and transchelation studies

In separate tubes, the ^{99m}Tc derivative (final ligand concentration 1 μM) was added to 900 μL of 1X phosphate-buffered saline solution (PBS), mouse serum, 1mM cysteine solution, 1mM histidine solution, or 1 mM DTPA solution. The samples were incubated at 37°C and analyzed by HPLC and ITLC after 1, 3 and 24 h.

Partition coefficient studies

Determination of log $P_{(o/w)}$ values was performed by the “shake-flask” method. To a solution containing 200 μL of octanol and 200 μL of water (obtained from a saturated octanol-water solution), 10 μL of 50 nM ^{99m}Tc(I)-estradiol-pyridin-2-yl hydrazine derivative was added. The resulting solution was vortexed at room temperature for 10 minutes and incubated at 37°C for

1 h. Aliquots (50 μL) were removed from the octanol and from the water phases, and the radioactivity measured in a Wallace Wizard 1480 automatic gamma counter.

Cell culture

ERα/β- and GPR30-expressing human breast adenocarcinoma MCF-7 cells (HTB 22; American Type Culture Collection, Rockville, MD) were cultured in Dulbecco's minimal essential medium containing fetal bovine serum (10%) and 100 units/mL penicillin and 100 μg/mL streptomycin. Cells were grown as a monolayer at 37°C, in a humidified atmosphere of 5% CO_2 and 95% air.

Receptor-binding studies

To evaluate ligand binding to the estrogen receptors expressed in MCF-7 cells, direct binding was performed with the ^{99m}Tc-labeled estradiol derivative. For saturation binding studies, 500,000 cells/tube in tissue culture medium were treated with increasing concentrations of the ^{99m}Tc-labeled estradiol derivative and incubated for 1 hour at 37°C. The cells were pelleted and washed three times with 1 mL phosphate-buffered saline (PBS). The radioactivity associated with the final pellet was counted using a Wallace Wizard 1480 automatic gamma counter. To determine nonspecific binding, the cells were incubated with 10 μM 17β-estradiol. To establish the affinity of the corresponding Re-labeled derivative (20), which serves as an isosteric non-radioactive surrogate for the ^{99m}Tc-labeled derivative (19,23), cells were treated with a trace amount of the radioligand and competition was carried out with increasing amounts of the Re-estradiol derivative. Binding data were analyzed using Graphpad Prism version 4 (San Diego, CA, USA).

Animal and tumor models

Animal use protocols were approved by the University of New Mexico Health Sciences Center Institutional Animal Care and Use Committee. To determine uptake during various stages of the estrous cycle, wild-type mature (8-10 weeks old) female C57BL/6 mice (Harlan Inc., Indianapolis, IN, USA) were used. Estrous cycle was determined by cytological examination of vaginal flushings (24). Mice used in this study were determined to be cycling by examination over 3-5 consecutive days prior to the day of the experiment.

Estrogen-dependent human breast adenocarcinoma MCF-7 tumors were generated by injecting 2-4 million MCF-7 cells subcutaneously in 8 week old female athymic NCr-nu/nu mice (NCI-Frederick, Frederick, MD, USA). One day prior to injection of the cells, a 60-day release 17β-estradiol (1.7 mg) pellet (Innovative Research of America, FL, USA) was implanted subcutaneously. After 6 weeks, tumors ranging from 0.6-0.9 cm in diameter were observed; at this stage, ovariectomy was performed and the pellet was removed. After a one-week recovery period, biodistribution and imaging studies were performed.

The collection and use of human tumor specimens was approved by the Human Research Review Committees (HRRC) at the University of New Mexico Health Sciences Center. Endometrial tumors were collected in cold sterile saline in the gross room of the Department of Pathology immediately after arrival from the operation room. Fresh patient tumor specimens were rinsed with cold sterile PBS and grossly necrotic tissue was trimmed away. The tumor was minced and rinsed with PBS again. Approximately 100 mg tumor suspended in 100 μl DMEM was injected subcutaneously into 8-week old athymic female NCr-nu/nu mice (25). Xenografted tumors were harvested before any dimension reached 20mm. The tumor used in this study was shown to be ER-positive by immunohistochemical staining (data not shown).

Biodistribution and SPECT/CT imaging studies

All mice were injected intravenously (tail vein) with the ^{99m}Tc-labeled estradiol derivative. To determine receptor specificity, 17β-estradiol (5 μg) was co-injected with the radiotracer. At the desired time point, the animals were sacrificed by CO_2 euthanasia. After sacrificing the animals, organs were carefully removed and isolated to determine the biodistribution characteristics of the tracer. The organ samples were weighed and the corresponding localized radioactivity was measured using an automated gamma counter after verifying the counting efficiency with standards. The percent injected dose per gram of tissue (%ID/g) and the percent injected dose per organ (%ID/organ) were calculated by comparison with standards representing the injected dose per animal.

NanoSPECT/CT imaging studies were performed using a multi-pinhole NanoSPECT/CT small animal imager (Bioscan Inc., Washington DC, USA). Whole body imaging studies were carried out on anesthetized animals using 1.5-2.0% isoflurane on a temperature controlled bed. The images were reconstructed, fused and analyzed using the InVivoScope software program (Bioscan Inc.). All animal experiments were conducted in compliance with the guidelines and approved protocols established by the Institutional Animal Care and Use Committee.

Statistical Analysis

All numerical data were expressed as the mean of the values ± the standard error of mean (S.E.M). Graphpad Prism version 4 (San Diego, CA, USA) was used for statistical analysis and a *P* value less that 0.05 was considered statistically significant.

RESULTS

Radiochemical purity

Preparation of the $[^{99m}Tc(CO)_3(H_2O)_3]^+$ "semi-aqua" intermediate was carried out yielding a radiochemical purity of > 95% (n > 30). The starting aqua ion $[^{99m}TcO_4]^-$ had a retention time of 0.9 min and the intermediate semi-aqua ion precursor had a retention time of 1.4 min. Over 85% of the $[^{99m}Tc(CO)_3(H_2O)_3]^+$ precursor was subsequently incorporated into the estradiol-pyridin-2-yl hydrazine derivative (Fig. 1). The pre-purification radiochemical purity assessed by HPLC was > 85% (n > 25) (Suppl. **Fig. 1A**). The two resolved radiometric peaks (4.1 and 5.2 min) likely represent the two diastereoisomeric chelates of the final product based on similar chromatographic profiles of the corresponding Re-labeled derivatives (20). Based on the HPLC analyses (and taking into account the elution profile of the ^{99m}Tc generator and the transient equilibrium between the parent and the daughter radionuclides), the calculated specific activity of the final product was approximately 47.5 TBq of ^{99m}Tc/mmol. The radiochemical purity was further improved to ≥ 95% by solid phase purification to remove excess ligand and unincorporated $[^{99m}Tc(CO)_3(H_2O)_3]^+$. Typical radiochemical yields after purification ranged from 60-80%.

Stability, transchelation and partition coefficient studies

The final ^{99m}Tc(I)-estradiol-pyridin-2-yl hydrazine derivative demonstrated high stability in buffer and mouse serum after 24 hours of incubation at 37°C (Table 1). Up to 30% transchelation was observed in the presence of a 1000-fold molar excess of histidine or cysteine after 24 hours of incubation at 37°C. The complex exhibited a log $P_{(o/w)}$ value of 3.9 ± 0.5 (n = 4) determined by shake flask method, compared to values of estradiol in the range of 3.3 to 5 (23).

Receptor binding studies

Direct intact cell binding studies were performed on ERα/β- and GPR30-expressing human breast adenocarcinoma MCF-7 cells. The ^{99m}Tc(I)-estradiol-pyridin-2-yl hydrazine derivative exhibited a dissociation constant (K_d) of 11 ± 1.5 nM with a calculated B_{max} of 1.3 ± 0.1 × 10^4 sites/cell (Fig. 2A), similar to previous estimates of the number of estrogen binding sites in these cells (21). The IC_{50} of the non-radioactive Re-conjugate (15 ± 1.4 nM, K_i=10.3 nM) was similar to the K_d of the ^{99m}Tc-conjugate (Fig. 2B). These values also compare well with our previous determinations with the Re-conjugate using competition of tritiated estrogen for purified ERα and a fluorescent estrogen for GPR30 in permeabilized cells where the relative binding affinities were 20% and 42%, respectively (20). The diastereoisomeric ^{99m}Tc(I)-estradiol-pyridin-2-yl hydrazine derivatives were separated by HPLC fractionation. Diastereoisomer A (retention time 4.1 min) exhibited a K_d of 12 ± 2.9 nM whereas diastereoisomer B (retention time 5.2 min) exhibited a K_d of 7.7 ± 2.6 nM.

Role of estrous cycle

Receptor-mediated uptake was observed in reproductive organs and the mammary gland in all stages of the estrous cycle (Table 2). The highest uptake of the tracer in reproductive organs and the mammary gland was observed in diestrus and the lowest uptake during estrus (Table 2). At 3 hours post-injection, the uptake in the mammary gland was 0.22 ± 0.02 % ID/g in estrus and increased to 1.31 ± 0.13 % ID/g in metestrus and 3.11 ± 0.24 % ID/g in diestrus. A similar trend of increasing uptake levels from estrus to metestrus and diestrus was found in uterus and ovaries. However, the uptake of the radiotracer by the ovaries was not significantly different between estrus (0.60 ± 0.06 %ID/g) and metestrus (0.76 ± 0.04 % ID/g). As shown in the Table 2, in bone, blood and muscle, the uptake was not receptor-mediated as there was no statistically significant difference in the values between unblocked and blocked treatments.

Biodistribution in non-tumor bearing C57Bl/6 animals in diestrus

The ^{99m}Tc-estradiol derivative demonstrated significant uptake in ER-expressing organs of interest with robust target tissue to muscle ratios in the range of 10:1 and moderate target tissue to blood ratios in the range of 1:1. In biodistribution studies, high liver uptake levels of 9.48% ID/g, 8.34% ID/g and 7.84% at 1 hr PI, 3 hr PI and 24 hr PI, respectively, probably resulted from high compound hydrophobicity (Table 3). Low uptake in the kidney and bladder at 1 and 3 hours PI suggested excretion occurred slowly via urine. At 3hr PI, approximately 5-10% ID was excreted in the feces and less than 2% ID was excreted in the urine. Urine and blood plasma was collected 3 hours PI and HPLC analysis was performed. No detectable radioactive metabolites were observed in the urine **(Suppl. Fig. 1B)** or plasma radiochromatograms **(Suppl. Fig. 1C)**.

Biodistribution in tumor-bearing animals

In tumor-bearing animals, in addition to receptor-mediated uptake in the estrogen-binding target organs, the ^{99m}Tc-estradiol derivative also displayed uptake in MCF-7 tumors and human primary endometrial tumors (Fig. 3). As in C57Bl/6 mice, high liver uptake values were obtained in animals bearing MCF-7 tumors (Fig. 4) and human primary endometrial tumors. High levels of radioactivity were again found in the feces. The uptake in the blood for MCF-7 tumor bearing animals was 1.25% ID/g, 2.03%ID/g and 0.81%ID/g at 1 hr PI, 3hr PI and 24 hr PI, respectively. Similarly, uptake in the blood was 1.27% ID/g, 1.59 %ID/g and 1.00% ID/g at 1 hr PI, 3hr PI and 24 hr PI, respectively. The target to muscle ratios were reasonably high to moderate ranging from 3.5 to 7.05 over the period of time; however, the target to blood ratios were poor and ranged from 0.3 to 1.0 (Table 4). At 3 hr PI, the tumor to muscle ratio was 5.67 and the tumor to blood ratio was 0.35. The tumor to muscle and tumor to blood ratios were

significantly reduced to 2.64 and 0.19, respectively, when blocking was performed with co-injection of 5 μg of 17β-estradiol.

Imaging studies

Imaging studies were carried out after injecting 18.5 MBq of the ^{99m}Tc(I)-estradiol-pyridin-2-yl hydrazine derivative via the tail vein. Whole body 60 s/projection imaging studies were carried out under anesthesia using a temperature controlled bed (36-38°C). In this study, very low counts were obtained in tumors and they were only visualized once the image threshhold was reduced to 2% maximum intensity. Whole body imaging studies also revealed high uptake in the liver and intestines (i.e. feces) (82.8 ± 1.9 % ID combined). Uptake in the MCF-7 tumor (3 hr PI) was relatively low (0.078 ± 0.010 % ID) when compared to the background. A focused 600 s/projection study was performed post-mortem for better visualization of the tumor to obtain higher counts. In this study, tumor visualization was better without significantly reducing the %ID scale (Fig. 5). In the reconstructed co-registered SPECT/CT maximum intensity projection image (Fig. 5A) and the reconstructed co-registered SPECT/CT sagittal slice (Fig. 5B), the radioactivity in the tumor and the liver can be visualized, whereas in the reconstructed co-registered SPECT/CT transverse slice (Fig. 5C) the localization of radioactivity can be visualized without any significant background.

DISCUSSION

Advances in molecular and cellular biology are transforming our understanding of basic physiology and pathology; similar advances in molecular imaging technologies now permit dynamic and quantitative studies *in vivo* with minimal invasiveness. In this study, we have developed a novel γ-emitting estradiol derivative and used it to investigate the interaction with estrogen receptors in defined stages of the estrous cycle in normal animals and also to evaluate its effectiveness in imaging mouse xenograft breast and endometrial tumors with SPECT.

Due to the desirable imaging characteristics of ^{99m}Tc, a number of groups have prepared ^{99m}Tc-labeled estradiol derivatives as breast cancer imaging agents. Most of the previously described ^{99m}Tc-labeled estradiol derivatives were modified at the 7α- and 17α-positions for incorporation of ^{99m}Tc (18,19). None of these reported steroidal analogues were successful as ideal imaging agents, due to either low binding affinity or the difficulty in preparing the labeled ^{99m}Tc with high specific activity and yields. However, it was observed that the analogues with the best characteristics were those substituted at the 17α-position. Based upon our previous characterization of 17α-substituted estradiol derivatives with respect to receptor binding and cell activation (20), we surmised that the use of an ethynyl group for linkage at the 17α-position would enhance receptor binding as well as cell permeability. Incorporation of a pyridyl moiety would allow for the incorporation of a [^{99m}Tc$(CO)_3(H_2O)_3$]+ group for production of an imaging agent. As a result, we prepared a neutral tridentate ^{99m}Tc(I) estradiol pyridin-2-yl hydrazine derivative using the tricarbonyl approach.

Due to the acid sensitivity of the tertiary propargylic 17β-alcohol of estradiol, the alkaline mixture was neutralized with acetic acid rather than HCl and heating was avoided to prevent elimination. Direct saturation binding studies were performed with the radioactive ^{99m}Tc-labeled derivative and competition binding studies were performed with the non-radioactive Re-labeled derivative on human breast adenocarcinoma MCF-7 cells. Performing receptor binding studies on whole cells with steroidal analogues poses challenges related to ligand equilibrium, the lipophilic nature of the ligand, estimation of free ligand, the processes of receptor activation and degradation and the presence of multiple estrogen receptor types, including GPR30 (26). As a result, careful consideration is required for data interpretation as one can easily over or under estimate the K_d. The ^{99m}Tc(I) estradiol pyridin-2-yl hydrazine derivative demonstrated a K_d of 11 ± 1.5 nM on MCF-7 cells, much higher than typically

reported values of estradiol itself (~ 0.1-1 nM, (27)) but comparable to the affinity of estrogen for GPR30 (~6 nM (26,28)). Furthermore, this K_d value is consistent with the affinities previously determined for Re-labeled derivative (20). Because chelate diastereoisomers demonstrated similar binding affinities *in vitro*, *in vivo* studies using separated diastereomers were not carried out. For *in vivo* evaluation, a mixture of diastereoisomers was injected in mature (8-10 weeks old) female C57BL/6 mice in defined stages of estrus cycle.

In studies with radiolabeled estrogen derivatives, it has been observed that the maximum uptake in the uterus is achieved during the diestrus phase (29,30); our finding that the highest uptake of ^{99m}Tc-labeled estrogen derivative in uterus, ovaries and mammary gland occurs during diestrus is consistent with these observations. Circulating estrogens are low during estrus, metestrus, and early diestrus. Then, towards late diestrus and into proestrus, just prior to ovulation, levels rise significantly. Available estrogen receptor concentration is determined by circulating estrogens, being reduced by ligand binding, but also being upregulated by estrogen-mediated receptor synthesis (31). Thus, at diestrus the combined conditions of minimal estrogen levels and maximum estrogen receptor levels, favor radiotracer uptake.

Another factor that may influence radiotracer uptake is hormonal regulation of the vasculature during the reproductive cycle. Blood flow to the ovaries, but not to the uterus is increased during estrus (32). However, uptake in the ovaries during estrus and metestrus was not significantly different (33). In addition, blood flow is not uniform in the left and right ovaries and therefore may affect experimental outcomes. In a recently published clinical study, endometrial standardized uptake values determined by FES PET imaging were significantly higher in the proliferative phase than in the secretory phase (34), highlighting the influence of menstrual cycle and endogenous estrogen levels in radiotracer uptake in humans.

Less is known about changes in the normal vasculature of the mammary gland; however, it has been observed that vascular permeability (but not blood flow or vascular density) is highest at diestrus (35). Importantly, the increase in vascular permeability at diestrus correlates with increased breast cancer growth rate and post-resection metastasis (35). Thus it is possible that the 14-fold increase in radiotracer uptake at diestrus is related to changes in vascular permeability. It would be worth investigating the possibility that elevated ligand availability during the luteal phase in women is linked to reduced 5-year disease-free survival in women with breast cancer who undergo mastectomy (along with tamixofen and oopherectomy) in the follicular phase as compared to the luteal phase (36). It should also be noted that not all human studies have found a difference in disease-free survival linked to the menstrual cycle (12).

The major goal for cancer imaging is accurate disease characterization through the application of functional and molecular imaging studies. FES PET cancer imaging has been immensely valuable to clinical oncologists for staging and visualizing primary and metastatic carcinomas (16,37). The supplemental molecular characterization and receptor-expression assessment of the tumor has often assisted in determining endocrine therapy options (12,13,38). As an alternative to PET imaging, we wanted to evaluate the utility of a ^{99m}Tc(I)-estradiol-pyridin-2-yl hydrazine derivative in SPECT imaging of breast and endometrial cancers. In previously published studies, problems encountered in developing a neutral Tc-estradiol derivative suitable for imaging of tumors were associated with excessive lipophilicity (i.e. logP values greater than 5 (23)) resulting in high liver and intestine uptake, low tumor to blood ratio and relatively low uptake in the tumor as compared to background (17-19). In our study, we encountered similar problems despite the fact that the logP value of our tracer was not significantly different from that previously reported for estradiol itself (3.9 *vs.* approx 3.7 (23), respectively). From biodistribution studies, uptake of the radiotracer in the tumor was receptor-mediated based on the significantly lower uptake upon co-injection with excess 17β-estradiol. Care must be taken while performing receptor blocking experiments with high doses

of 17β-estradiol as estrogen alters vascular physiology, blood flow and receptor expression levels (39). Consequently, when the blocking dose was injected 1 hour prior to the injection of the radiotracer, we observed higher uptake in organs such as liver and lungs.

In this study, we chose the MCF-7 tumor model as representative of estrogen-dependent carcinomas; however, this model requires estrogen supplementation, which creates additional technical challenges involving ovariectomy and estrogen supplementation with pellets. For example, when we performed radiotracer studies 3 days after removing the estrogen pellet and the ovaries, the uptake in target organs was not blocked by excess ligand, likely due to high endogenous levels of estrogen. It is also known that estrogen supplementation and pregnancy can elevate the levels of sex steroid-binding protein and alpha-fetoprotein, which result in lower target to blood ratios (30). Our studies revealed that a period of at least 8 days following pellet and ovary removal was required to obtain significant results, though oophorectomy is not typically an option in the clinical setting. The low level of tracer uptake in tumor compounded with a high background resulted in poor whole-body SPECT/CT images using 60 s/ projection. The image quality was greatly improved when a focused study was performed with 600 s/ projection (Fig. 6). As a proof of principle, we have demonstrated that the tracer localizes in the tumor; however, such long acquisition time studies may not be feasible in clinical settings.

Currently, there are no readily available and easily synthesized SPECT imaging agents for assessing reproductive cancers expressing estrogen-binding activity. Despite the challenges and drawbacks, newer ^{99m}Tc-based estradiol derivatives have been reported, including the one in this study. However, to date all of them have failed to provide an alternative to FES and PET, mainly due to low tumor uptake compounded with high background levels. To overcome the problems posed by such steroidal analogues, we propose the development of neutral non-steriodal analogues that would specifically bind to each estrogen receptor subtype (ERα, ERβ and GPR30) with high affinity (28,40).

CONCLUSION

In conclusion, in our current study, highest target-uptakes were observed during diestrus consistent with differential expression of ER and estrogen levels during the estrous cycle. Although the ^{99m}Tc(I)-estradiol-pyridin-2-yl hydrazine derivative showed encouraging results in standard biodistribution studies, as it demonstrated receptor-mediated uptake in normal target organs as well as human breast adenocarcinoma MCF-7 tumors and primary human endometrial tumors, further structural modifications are needed to optimize these compounds for improved imaging characteristics.

ACKNOWLEDGEMENTS

This study was supported by NIH grants CA116662 and CA127731 (ERP), NIH grant SCORE GM08136 (JBA), NIH grant MH074425 (LAS), the University of New Mexico Cancer Research and Treatment Center (NIH P30 CA118100), the New Mexico Cowboys for Cancer Research Foundation, the Oxnard Foundation and the Stranahan Foundation. Images in this paper were generated in the Keck-UNM Small Animal Imaging resource established with funding from the W.M Keck Foundation. The technical assistance of Tamara Anderson and Kamalika Nag is greatly appreciated. We thank Dr. Robert Atcher (Biosciences Division, Los Alamos National Laboratory) for his valuable insights and Dr. Mary Dyszlewski (Mallinckrodt, Tyco Healthcare, USA) for providing the Isolink® kits.

References

1. Jemal A, Siegel R, Ward E, et al. Cancer statistics, 2006. CA Cancer J Clin 2006;56:106–130. [PubMed: 16514137]
2. Yager JD, Davidson NE. Estrogen carcinogenesis in breast cancer. N Engl J Med 2006;354:270–282. [PubMed: 16421368]

3. Filardo EJ, Graeber CT, Quinn JA, et al. Distribution of GPR30, a seven membrane-spanning estrogen receptor, in primary breast cancer and its association with clinicopathologic determinants of tumor progression. Clin Cancer Res 2006;12:6359–6366. [PubMed: 17085646]
4. Smith HO, Leslie KK, Singh M, et al. GPR30: a novel indicator of poor survival for endometrial carcinoma. Am J Obstet Gynecol 2007;196(386):e381–389.
5. Jordan CV, Lewis-Wambi J, Kim H, et al. Exploiting the apoptotic actions of oestrogen to reverse antihormonal drug resistance in oestrogen receptor positive breast cancer patients. Breast. 2007in press
6. Bafaloukos D. Neo-adjuvant therapy in breast cancer. Ann Oncol 2005;16(Suppl 2):ii174–181. [PubMed: 15958453]
7. Veronesi U, Boyle P, Goldhirsch A, Orecchia R, Viale G. Breast cancer. Lancet 2005;365:1727–1741. [PubMed: 15894099]
8. Katzenellenbogen JA, Welch MJ, Dehdashti F. The development of estrogen and progestin radiopharmaceuticals for imaging breast cancer. Anticancer Research 1997;17:1573–1576. [PubMed: 9179196]
9. Vollenweider-Zerargui L, Barrelet L, Wong Y, Lemarchand-Beraud T, Gomez F. The predictive value of estrogen and progesterone receptors' concentrations on the clinical behavior of breast cancer in women. Clinical correlation on 547 patients. Cancer 1986;57:1171–1180. [PubMed: 3943040]
10. Landvatter SW, Kiesewetter DO, Kilbourn MR, Katzenellenbogen JA, Welch MJ. (2R*, 3S*)-1-[18F]fluoro-2,3-bis(4-hydroxyphenyl)pentane [(18F]fluoronor-hexestrol), a positron-emitting estrogen that shows highly-selective, receptor-mediated uptake by target tissues in vivo. Life Sciences 1983;33:1933–1938. [PubMed: 6316052]
11. Mathias CJ, Welch MJ, Katzenellenbogen JA, et al. Characterization of the uptake of 16 alpha-([18F] fluoro)-17 beta-estradiol in DMBA-induced mammary tumors. International Journal of Radiation Applications and Instrumentation. 1987;14:15–25.
12. Linden HM, Stekhova SA, Link JM, et al. Quantitative fluoroestradiol positron emission tomography imaging predicts response to endocrine treatment in breast cancer. J Clin Oncol 2006;24:2793–2799. [PubMed: 16682724]
13. Mortimer JE, Dehdashti F, Siegel BA, Katzenellenbogen JA, Fracasso P, Welch MJ. Positron emission tomography with 2-[18F]Fluoro-2-deoxy-D-glucose and 16alpha-[18F]fluoro-17beta-estradiol in breast cancer: correlation with estrogen receptor status and response to systemic therapy. Clin Cancer Res 1996;2:933–939. [PubMed: 9816253]
14. Hecht JL, Mutter GL. Molecular and pathologic aspects of endometrial carcinogenesis. J Clin Oncol 2006;24:4783–4791. [PubMed: 17028294]
15. Shang Y. Molecular mechanisms of oestrogen and SERMs in endometrial carcinogenesis. Nat Rev Cancer 2006;6:360–368. [PubMed: 16633364]
16. Yoshida Y, Kurokawa T, Sawamura Y, et al. The positron emission tomography with F18 17beta-estradiol has the potential to benefit diagnosis and treatment of endometrial cancer. Gynecol Oncol 2007;104:764–766. [PubMed: 17156828]
17. Bigott HM, Parent E, Luyt LG, Katzenellenbogen JA, Welch MJ. Design and synthesis of functionalized cyclopentadienyl tricarbonylmetal complexes for technetium-94m PET imaging of estrogen receptors. Bioconjugate chemistry 2005;16:255–264. [PubMed: 15769078]
18. Luyt LG, Bigott HM, Welch MJ, Katzenellenbogen JA. 7alpha- and 17alpha-substituted estrogens containing tridentate tricarbonyl rhenium/technetium complexes: synthesis of estrogen receptor imaging agents and evaluation using microPET with technetium-94m. Bioorg Med Chem 2003;11:4977–4989. [PubMed: 14604660]
19. Skaddan MB, Wust FR, Jonson S, et al. Radiochemical synthesis and tissue distribution of Tc-99m-labeled 7alpha-substituted estradiol complexes. Nuclear Medicine and Biology 2000;27:269–278. [PubMed: 10832084]
20. Ramesh C, Bryant B, Nayak T, et al. Linkage effects on binding affinity and activation of GPR30 and estrogen receptors ERalpha/beta with tridentate pyridin-2-yl hydrazine tricarbonyl-Re/(99m)Tc (I) chelates. J Am Chem Soc 2006;128:14476–14477. [PubMed: 17090028]
21. Hochberg RB, Rosner W. Interaction of 16 alpha-[125I]iodo-estradiol with estrogen receptor and other steroid-binding proteins. Proc Natl Acad Sci U S A 1980;77:328–332. [PubMed: 6928625]

22. Murphy BE. Binding of testosterone and estradiol in plasma. Can J Biochem 1968;46:299–302. [PubMed: 5690431]
23. Skaddan MB, Wust FR, Katzenellenbogen JA. Synthesis and Binding Affinities of Novel Re-Containing 7alpha-Substituted Estradiol Complexes: Models for Breast Cancer Imaging Agents. J Org Chem 1999;64:8108–8121. [PubMed: 11674724]
24. Nelson JF, Felicio LS, Randall PK, Sims C, Finch CE. A longitudinal study of estrous cyclicity in aging C57BL/6J mice: I. Cycle frequency, length and vaginal cytology. Biol Reprod 1982;27:327–339. [PubMed: 6889895]
25. Dai D, Albitar L, Nguyen T, Laidler LL, Singh M, Leslie KK. A therapeutic model for advanced endometrial cancer: systemic progestin in combination with local adenoviral-mediated progesterone receptor expression. Molecular cancer therapeutics 2005;4:169–175. [PubMed: 15657363]
26. Revankar CM, Cimino DF, Sklar LA, Arterburn JB, Prossnitz ER. A transmembrane intracellular estrogen receptor mediates rapid cell signaling. Science 2005;307:1625–1630. [PubMed: 15705806]
27. Kuiper GG, Carlsson B, Grandien K, et al. Comparison of the ligand binding specificity and transcript tissue distribution of estrogen receptors alpha and beta. Endocrinology 1997;138:863–870. [PubMed: 9048584]
28. Bologa CG, Revankar CM, Young SM, et al. Virtual and biomolecular screening converge on a selective agonist for GPR30. Nat Chem Biol 2006;2:207–212. [PubMed: 16520733]
29. De Hertogh R, Ekka E, Vanderheyden I, Hoet JJ. In vivo observation on cyclic variations of estradiol-17beta,6,7-3H uptake by the uterus of the adult rat. Endocrinology 1971;88:175–179. [PubMed: 5099583]
30. McElvany KD, Carlson KE, Katzenellenbogen JA, Welch MJ. Factors affecting the target site uptake selectivity of estrogen radiopharmaceuticals: serum binding and endogenous estrogens. J Steroid Biochem 1983;18:635–641. [PubMed: 6191127]
31. Brenner RM, West NB. Hormonal regulation of the reproductive tract in female mammals. Annu Rev Physiol 1975;37:273–302. [PubMed: 164819]
32. Dowell RT, Gairola CG, Diana JN. Reproductive organ blood flow measured using radioactive microspheres in diestrous and estrous mice. Am J Physiol 1992;262:R666–670. [PubMed: 1566933]
33. Silberstein GB, Van Horn K, Hrabeta-Robinson E, Compton J. Estrogen-triggered delays in mammary gland gene expression during the estrous cycle: evidence for a novel timing system. J Endocrinol 2006;190:225–239. [PubMed: 16899557]
34. Tsuchida T, Okazawa H, Mori T, et al. In vivo imaging of estrogen receptor concentration in the endometrium and myometrium using FES PET--influence of menstrual cycle and endogenous estrogen level. Nucl Med Biol 2007;34:205–210. [PubMed: 17307128]
35. Wood PA, Bove K, You S, Chambers A, Hrushesky WJ. Cancer growth and spread are saltatory and phase-locked to the reproductive cycle through mediators of angiogenesis. Molecular cancer therapeutics 2005;4:1065–1075. [PubMed: 16020664]
36. Love RR, Duc NB, Dinh NV, et al. Mastectomy and oophorectomy by menstrual cycle phase in women with operable breast cancer. Journal of the National Cancer Institute 2002;94:662–669. [PubMed: 11983754]
37. McGuire AH, Dehdashti F, Siegel BA, et al. Positron tomographic assessment of 16 alpha-[18F] fluoro-17 beta-estradiol uptake in metastatic breast carcinoma. J Nucl Med 1991;32:1526–1531. [PubMed: 1869973]
38. Bennink RJ, van Tienhoven G, Rijks LJ, Noorduyn AL, Janssen AG, Sloof GW. In vivo prediction of response to antiestrogen treatment in estrogen receptor-positive breast cancer. J Nucl Med 2004;45:1–7. [PubMed: 14734659]
39. Haas E, Meyer MR, Schurr U, et al. Differential effects of 17beta-estradiol on function and expression of estrogen receptor alpha, estrogen receptor beta, and GPR30 in arteries and veins of patients with atherosclerosis. Hypertension 2007;49:1358–1363. [PubMed: 17452498]
40. Revankar CM, Mitchell HD, Field AS, et al. Synthetic estrogen derivatives demonstrate the functionality of intracellular GPR30. ACS Chem Biol 2007;2:536–544. [PubMed: 17655271]

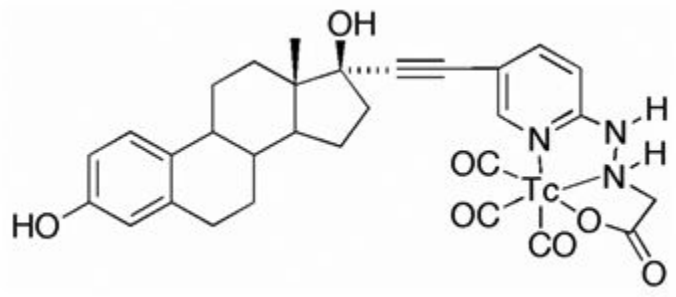

Figure 1.
Chemical structure the of ^{99m}Tc(I)-estradiol-pyridin-2-yl hydrazine derivative possessing an alkyne linkage and prepared by the tri-carbonyl approach.

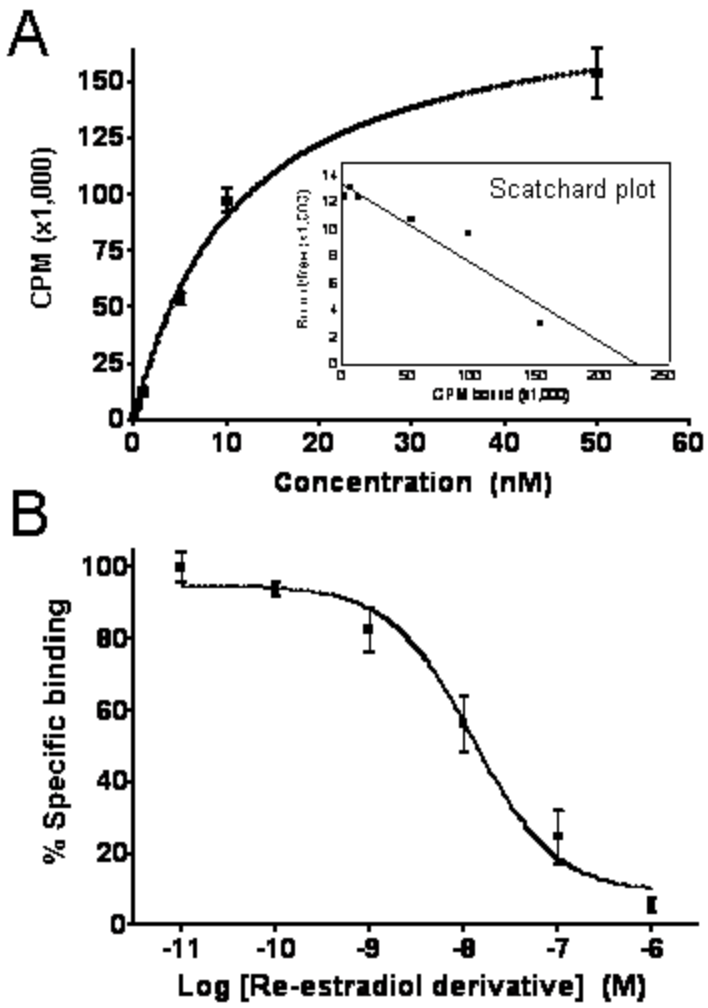

Figure 2.

(A) Saturation binding curve with inset Scatchard plot of radioligand receptor binding studies performed with ^{99m}Tc(I)-estradiol-pyridin-2-yl hydrazine derivative on MCF-7 human breast adenocarcinoma cells. The ^{99m}Tc(I)-estradiol-pyridin-2-yl hydrazine derivative showed a K_d of 11.0 ± 1.5 nM and B_{max} of 1.3 ± 0.1 × 10^4 sites/cell. **(B)** Competition binding curve from radioligand receptor binding studies performed with the ^{99m}Tc(I)-estradiol-pyridin-2-yl hydrazine derivative as the radiotracer and the corresponding non-radioactive Re-labeled derivative as competitior using MCF-7 cells. The non-radioactive Re-estradiol-pyridin-2-yl hydrazine derivative yielded an IC_{50} of 15.0 ± 1.5 nM and a calculated K_i of 10.3 nM. Values were determined from three independent experiments.

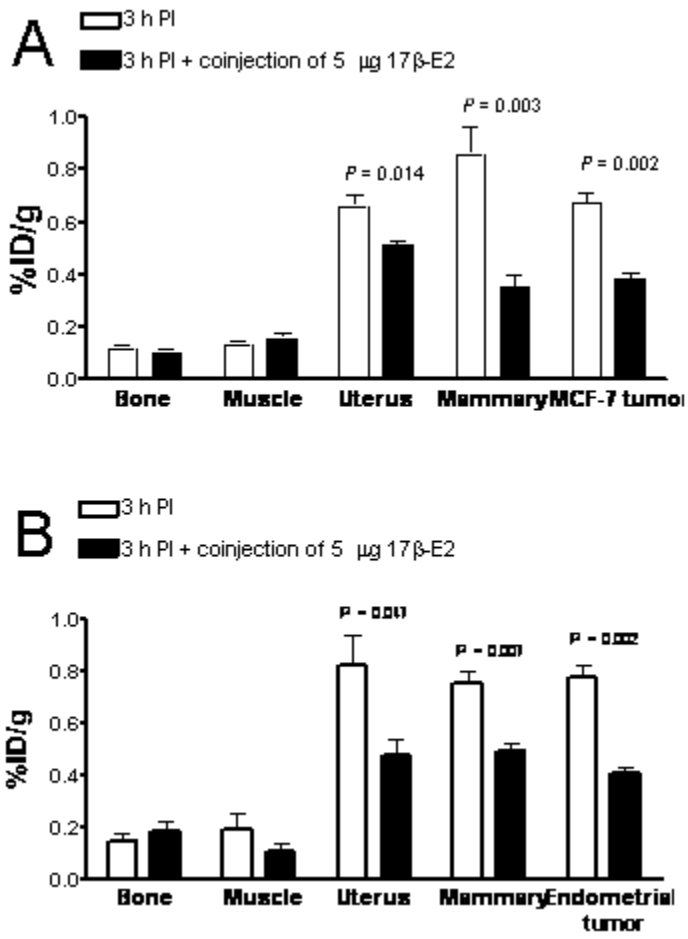

Figure 3.

Receptor-mediated uptake of the ^{99m}Tc(I)-estradiol-pyridin-2-yl hydrazine derivative in ovariectomized female athymic (NCr) nu/nu bearing **(A)** MCF-7 human breast adenocarcinoma tumors or **(B)** human primary endometrial tumors. Uptake values are expressed as % ID/g and were determined by biodistribution studies. Data represent the mean value ± SEM from at least three determinations.

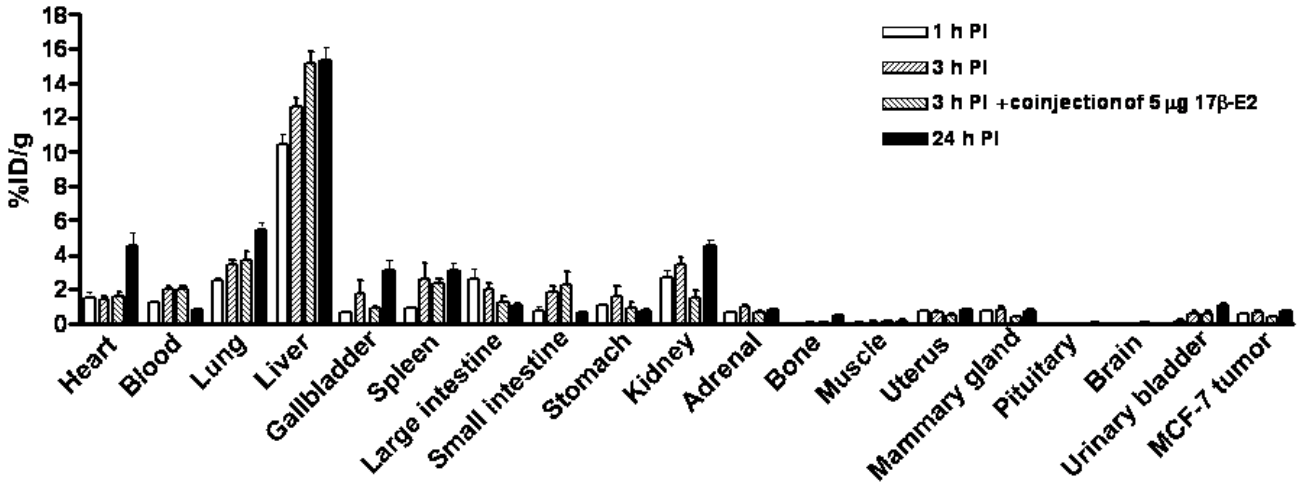

Figure 4.

Uptake values of the ^{99m}Tc(I)-estradiol-pyridin-2-yl hydrazine derivative in selected organs of ovariectomized female athymic (NCr) nu/nu mice bearing MCF-7 human breast adenocarcinoma tumors. Biodistribution data was obtained at 1, 3 and 24 hr PI. All uptake values are expressed at % ID/g. Data represent the mean value ± SEM from at least four determinations.

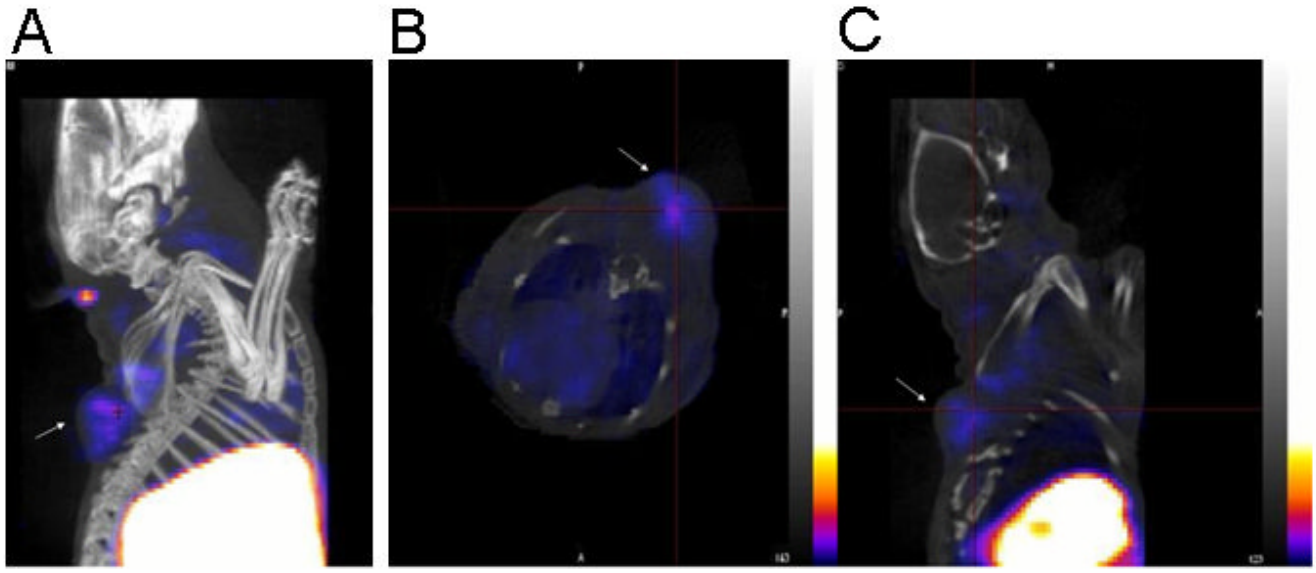

Figure 5.

(A) Reconstructed co-registered maximum intensity projection (MIP) SPECT/CT image. **(B)** Reconstructed co-registered transverse SPECT/CT slice image. **(C)** Reconstructed co-registered sagittal SPECT/CT slice image. In all images the tumor is shown with an arrow. The images were acquired from an ovariectomized female athymic (NCr) nu/nu mouse bearing an MCF-7 human breast adenocarcinoma tumor bearing mice injected with approximately 18.5 MBq of ^{99m}Tc(I)-estradiol-pyridin-2-yl hydrazine derivative via tail vein. The image was acquired 3 hr PI post-mortem. For the SPECT image, a focused scan of 600 s/projection was used; the CT image was acquired with 180 projections (1.5 pitch and an energy of 45 kVp). The energy window for SPECT acquisition of ^{99m}Tc was set at 140 ± 14 keV. The images were reconstructed, fused and analyzed using InVivoScope software program (Bioscan Inc, Washington DC, USA). In these representative SPECT images, the maximum intensity of the color scale was set to 25%.

Table 1

Stability of the ^{99m}Tc(I)-estradiol-pyridin-2-yl hydrazine derivative

Time	1 mM Histidine	1 mM Cysteine	1 mM DTPA	PBS	C57Bl/6 serum
1 hr	88.8 ± 0.7 [a]	89.2 ± 0.4	97.6 ± 0.2	97.4 ± 0.5	97.4 ± 0.6
3 hr	86.9 ± 0.4	84.7 ± 2.2	95.2 ± 0.9	96.1 ± 1.2	95.5 ± 1.1
24 hr	76.3 ± 2.8	68.2 ± 2.7	92.0 ± 4.0	97.3 ± 1.4	93.9 ± 2.3

[a]Samples were incubated at 37°C in 1 mM histidine, 1 mM cysteine, 1 mM DTPA, phosphate buffer saline and C57Bl/6 serum. The stability was assessed by HPLC and ITLC and all values stated in the table are % stability. Data represent the mean value ± SEM from three determinations.

Table 2

Uptake values of ^{99m}Tc(I)-estradiol-pyridin-2-yl hydrazine derivative throughout the estrous cycle

Reproductive organs, mammary glands, bone, blood and muscle of 8-10 weeks old female C57Bl/6 mice in defined stages of estrous cycle were evaluated. All uptake values are expressed as % ID/g and were determined from biodistribution studies. Data represent the mean value ± SEM from 4 determinations.

Organ	Estrus	Estrus (block)[a]	Metestrus	Metestrus(block)[a]	Diestrus	Diestrus (block)[a]
Blood	2.30 ± 1.02	1.92 ± 0.95	2.50 ± 0.88	2.54 ± 1.63	2.70 ± 0.12	2.42 ± 0.24
Bone	0.22 ± 0.06	0.17± 0.02	0.15 ± 0.04	0.24 ± 0.10	0.14 ± 0.01	0.17 ± 0.02
Muscle	0.09± 0.01	0.09 ± 0.02	0.11 ± 0.01	0.08 ± 0.04	0.15 ± 0.02	0.13 ± 0.02
Mammary[b,c]	0.22 ± 0.02	0.08 ± 0.01	1.31 ± 0.13	0.19 ± 0.02	3.11 ± 0.24	0.78 ± 0.06
Uterus[b, c]	0.55 ± 0.02	0.36 ± 0.02	0.79 ± 0.09	0.48 ± 0.04	1.44 ± 0.07	0.63 ± 0.04
Ovaries[b, d]	0.60 ± 0.06	0.24 ± 0.03	0.76 ± 0.04	0.39 ± 0.05	1.24 ± 0.22	0.60 ± 0.05

[a] Receptor blocking studies were performed by co-injecting 5 μg 17β-estradiol with the radiotracer.

[b] Uptake values ($n \geq 4$) in each phase of the estrous cycle are significantly different ($p < 0.05$) from the values in the same phase of the estrous cycle when compared to uptake in the presence of 5 μg co-injected17β-E2.

[c] Uptake values ($n \geq 4$) in each phase of the estrous cycle are significantly different ($p < 0.05$) from one another.

[d] Uptake values ($n \geq 4$) in each phase of the estrous cycle are not significantly different ($p < 0.05$) from one another comparing the estrus and metestrus, or the metestrus and diestrus. However, the values are significantly different comparing estrus and diestrus.

Table 3

Time-dependent uptake of ^{99m}Tc(I)-estradiol-pyridin-2-yl hydrazine derivative

Biodistribution of the ^{99m}Tc(I)-estradiol-pyridin-2-yl hydrazine derivative in selected organs of 8-10 weeks old female C57Bl/6 mice in diestrus. All uptake values ($n \geq 6$) are expressed as % ID/g. Data represent the mean value ± SEM from at least 6 determinations.

Organ	1 hour PI	3 hour PI	24 hour PI
Kidney	1.70 ± 0.33	1.31 ± 0.06	1.19 ± 0.12
Adrenal	1.87 ± 0.75	3.10 ± 0.46	0.58 ± 0.15
Heart	1.17 ± 0.23	1.61 ± 0.51	0.86 ± 0.12
Small Intestine	0.44 ± 0.20	1.87 ± 0.54	0.68 ± 0.05
Large Intestine	0.28 ± 0.06	3.24 ± 0.95	0.89 ± 0.19
Liver	9.48 ± 0.99	8.34 ± 0.18	7.84 ± 0.24
Urinary Bladder	0.19 ± 0.05	0.96 ± 0.27	5.99 ± 4.34
Blood	2.47 ± 0.07	2.79 ± 0.21	1.02 ± 0.39
Bone	0.28 ± 0.16	0.14 ± 0.01	0.85 ± 0.53
Lung	1.49 ± 0.39	1.12 ± 0.19	0.83 ± 0.17
Stomach	0.85 ± 0.14	1.08 ± 0.37	0.34 ± 0.04
Muscle	0.10 ± 0.01	0.18 ± 0.03	0.35 ± 0.10
Mammary	1.21 ± 0.26	3.07 ± 0.40	1.59 ± 0.59
Uterus	1.32 ± 0.37	1.48 ± 0.10	1.60 ± 0.17
Ovaries	1.40 ± 0.32	1.19 ± 0.26	0.97 ± 0.25
Brain	0.06 ± 0.01	0.10 ± 0.01	0.02 ± 0.01

Table 4

Target to muscle and target to blood ratios of ^{99m}Tc(I)-estradiol-pyridin-2-yl hydrazine derivative

^{99m}Tc(I)-estradiol-pyridin-2-yl hydrazine uptake was determined in ovariectomized female athymic NCr-nu/nu mice bearing MCF-7 human breast adenocarcinoma tumors. Data represent the mean value ± SEM from at least 4 determinations.

Target/Background	1 hour PI	3 hour PI	3 hour PI (block)[a,b]	24 hour PI
Uterus/Muscle	6.44 ± 0.81	5.21 ± 1.12	3.32 ± 0.46	3.58 ± 0.47
Mammary/Muscle	7.05 ± 0.87	6.74 ± 1.21	2.45 ± 0.51	3.50 ± 0.82
MCF-7 tumor/Muscle	4.75 ± 0.43	5.67 ± 1.06	2.64 ± 0.53	3.54 ± 0.26
Uterus/Blood	0.57 ± 0.02	0.34 ± 0.04	0.24 ± 0.02	1.02 ± 0.16
Mammary/Blood	0.62 ± 0.05	0.43 ± 0.05	0.18 ± 0.02	0.91 ± 0.11
MCF-7 tumor/Blood	0.43 ± 0.07	0.35 ± 0.05	0.19 ± 0.02	1.03 ± 0.19

[a] All ratios at 3 hr PI are significantly different ($p < 0.05$) from the ratios at 3 hr PI when the radiotracer was co-injected with 5 μg of 17ß-E2 for blocking the receptor.

[b] Receptor blocking studies were performed by co-injecting 5 μg 17β-estradiol with the radiotracer.